

Article ID: 1001-3555(2017)03-0206-09

## Modification of Wüstite Based Ammonia Synthesis Catalyst With Fine Fe particles

LI Lei, HAN Wen-feng\*, LI Lin-hui, LIU Hua-zhang\*

(Institute of Industrial Catalysis, Zhejiang University of Technology, Hangzhou 310032, China)

**Abstract:** Commercial and pre-reduced wüstite based catalyst was modified by nano and micro Fe particles via in-situ solid-state reaction of  $\text{Fe}(\text{NO})_3 \cdot 9\text{H}_2\text{O}$  with  $\text{H}_2\text{C}_2\text{O}_4 \cdot 2\text{H}_2\text{O}$  at room temperature, and the as-prepared samples were characterized by means of XRD, SEM, TG-DTG,  $\text{H}_2$ -TPR. The solid-state reaction of  $\text{Fe}(\text{NO}_3)_3 \cdot 9\text{H}_2\text{O}$  with  $\text{H}_2\text{C}_2\text{O}_4 \cdot 2\text{H}_2\text{O}$  at room temperature yields  $\text{Fe}_2(\text{C}_2\text{O}_4)_3 \cdot 5\text{H}_2\text{O}$  completely and disperses on the surface of iron catalyst. With modification, significant improvement in ammonia synthesis activity of the catalysts was observed. With the Fe loading of 5%, ammonia concentrations at the outlet of the reactor are improved from 12.4% to 15.6% at 450 °C, 11.0% to 14.8% at 425 °C and 9.4% to 13% at 400 °C, respectively. Via simple and one-step modification (solid-state reaction), the activity of iron is enhanced by 25% to 38%. Following calcination or reduction, the formed  $\text{Fe}_{1-x}\text{O}$  or Fe particles interact with the surface of iron catalyst strongly, which stabilizes the nano and micro particles during reaction. As a result, high stability of catalyst is achieved.

**Key words:** ammonia synthesis; solid-state reaction; wüstite; modification; ionic oxalate

**CLC number:** O643.32      **Document code:** A

Ammonia synthesis reaction plays a key role in the development of heterogeneous catalysis and related industries. Magnetite based catalyst with  $\text{Fe}_3\text{O}_4$  as precursor has been investigated for more than 100 years and no further significant improvement are expected<sup>[1-2]</sup>. However, in 1986, we discovered a novel wüstite-based catalyst with  $\text{Fe}_{1-x}\text{O}$  as the precursor of the catalyst<sup>[3]</sup>. This catalyst shows high activity, high reducibility and has been applied to various ammonia plants. As reported, it presents complete performance with Ru/C catalysts<sup>[4]</sup>.

Recently, most work has been focused on the development of non-Fe catalysts, such as Ru/C<sup>[5-7]</sup> or new carrier materials for Ru catalysts<sup>[8-10]</sup>. In addition, cobalt promoted with other metals<sup>[11-13]</sup> was suggested to be the potential catalyst for ammonia synthesis. Relatively little work centers around the improvement on the iron based catalysts. As we all know, the cost of iron catalysts is much lower than other cata-

lysts. Therefore, we suggest that modification and enhancement of the existing iron catalysts are worth noting.

In iron based catalysts, promoters play major role in the performance of catalysts<sup>[14]</sup>. Actually, wüstite precursor is favourable for the dispersion of  $\text{Al}_2\text{O}_3$  and MgO promoters<sup>[15]</sup>. Although almost all the elements in the periodical table have been explored, still there are reports on new promoters. In addition to the well consolidated promoters, such as oxide of potassium, magnesium and aluminium, lithium, rare earth gangue and niobium oxide were found to be potential promoters for iron catalysts<sup>[16-19]</sup>. Interestingly, photoprompted hot electrons were found to be effective for ammonia synthesis even under atmospheric pressure<sup>[20]</sup>. It was confirmed that plasmonic metal nanoparticles can not only generate highly reactive electrons and holes but also induce resonant surface excitations through plasmonic decay, which can catalyze dissociation and redox reac-

**Received date:** 2017-03-01; **Revised date:** 2017-04-20.

**First author:** LI Lei (1991-), Female, Master degree, E-mail: llihuagong@163.com.

**Corresponding author:** Tel:15150874035, E-mail: hanwf@zjut.edu.cn (W. H.); cuihua@zjut.edu.cn (H. L.).

tions under mild conditions<sup>[21]</sup>.

It is well accepted that ammonia synthesis reaction is structure sensitive over iron and ruthenium catalysts<sup>[22-24]</sup>. The crystallite size and shapes have significant effect on the activity of catalyst. With the increase of crystallite size, rate of ammonia decomposition over Fe surface decreases dramatically<sup>[25-26]</sup>. Size-dependent transformation of  $\alpha$ -Fe into  $\gamma$ -Fe<sub>4</sub>N was also observed<sup>[27]</sup>. In addition, as iron based catalysts are usually prepared by fusing process, the surface is relatively smooth and the surface area is low. Hence, improvement of surface roughness is helpful for the activity of catalyst<sup>[28]</sup>.

Surprisingly, high-energy ball-milling is a potential route for the preparation of iron catalysts for ammonia synthesis<sup>[29]</sup>. By ball-milling of either oxide components or commercial iron catalyst, the activity increased slightly. We suggest that nano and micro iron and iron oxides produced during ball-milling modifies the surface of catalyst and contribute to the activity.

In the present study, we propose a simple and efficient way to modify the commercial pre-reduced wüstite based catalyst with nano and micro Fe particles. The preparation of nano and micro Fe particles and modification of pre-reduced wüstite based catalyst

was fulfilled via the in-situ solid-state reaction at room temperature.

## 1 Materials and Methods

### 1.1 Preparation of Fe<sub>2</sub>(C<sub>2</sub>O<sub>4</sub>)<sub>3</sub> · 5H<sub>2</sub>O

Fe(NO<sub>3</sub>)<sub>3</sub> · 9H<sub>2</sub>O (from Guangdong Guanghua Sci-Tech Co. Ltd.) and H<sub>2</sub>C<sub>2</sub>O<sub>4</sub> · 2H<sub>2</sub>O (from Shanghai Lingfeng Chemical Reagent Co. Ltd.) were analytical grade reagents and used as received. According to the molar ratio of Fe(NO<sub>3</sub>)<sub>3</sub> · 9H<sub>2</sub>O and oxalic acid = 2 : 3, desired weight of Iron(III) nitrate nonahydrate (Fe(NO<sub>3</sub>)<sub>3</sub> · 9H<sub>2</sub>O) and oxalic acid (H<sub>2</sub>C<sub>2</sub>O<sub>4</sub> · 2H<sub>2</sub>O) were prepared. Then, Fe(NO<sub>3</sub>)<sub>3</sub> · 9H<sub>2</sub>O and H<sub>2</sub>C<sub>2</sub>O<sub>4</sub> · 2H<sub>2</sub>O were milled into fine powder, respectively. And then fine Fe(NO<sub>3</sub>)<sub>3</sub> · 9H<sub>2</sub>O powder was well mixed with fine oxalic acid powder in an agate mortar. During the milling, pungent gases were emitted. Subsequently, the homogeneous mixture was transferred into a beaker, and then dried at 110 °C for 5 h. Finally, the product was collected for structure and property characterization.

### 1.2 Preparation of catalyst

The detailed process is illustrated in Fig. 1. According to the Fe(NO<sub>3</sub>)<sub>3</sub> · 9H<sub>2</sub>O / H<sub>2</sub>C<sub>2</sub>O<sub>4</sub> · 2H<sub>2</sub>O feed mole ratio and Fe loading, desired weight of pre-

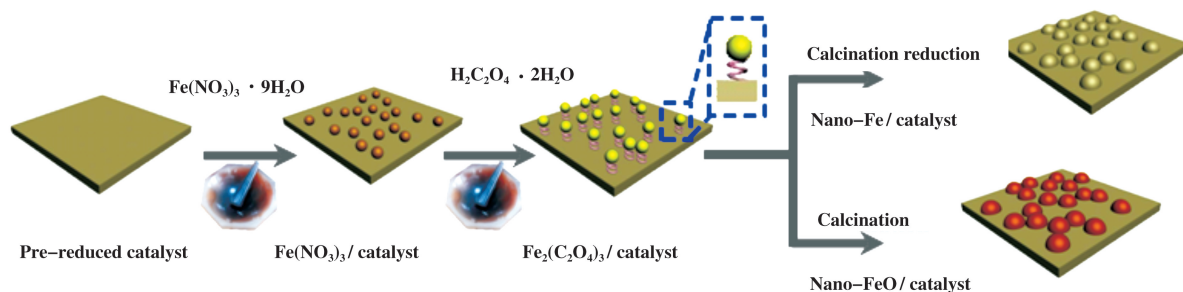


Fig. 1 Schematic illustration of modification of pre-reduced wüstite based catalyst with nano and micro Fe particles via solid-state reaction

reduced wüstite based catalyst (0.4 ~ 0.8 mm) was well mixed with fine Fe(NO<sub>3</sub>)<sub>3</sub> · 9H<sub>2</sub>O powder in an agate mortar. Then, desired amounts of fine oxalic acid powder were introduced into the mortar and milled for 30 min. During the milling, pungent gases were emitted. Finally, the sample was dried at 110 °C for 5 h. Prior to the activity tests, the modified catalysts

were subject to calcination at 400 ~ 450 °C or in-situ calcination and reduction at the same temperature.

### 1.3 Catalysts characterization

To investigate the morphology of the catalysts, SEM performed on a Hitachi S-4700 (II) electron microscope (Tokyo, Japan) with an accelerating voltage of 15 kV was used. The samples were gold coated by

cathodic sputtering.

The crystal phases of the catalysts were analyzed by powder X-ray diffraction (XRD), using a PANalytical X'Pert Pro diffractometer (Cu K $\alpha$  radiation,  $\lambda = 0.154\ 056\ \text{nm}$ ,  $2\theta = 10^\circ \sim 80^\circ$ ).

Thermogravimetric analysis in argon (Ar-TG) was conducted on NETZSCH-STA449C. Weight about 10 mg catalyst (particle size 0.154 ~ 0.050 mm) and heat it to 700 °C at a heating rate of 10 °C/min under argon with the flow rate of 30 mL/min.

Temperature programmed reduction (TPR) profiles of samples (weight about 30 mg catalyst) were generated on a PX200 catalyst characterization instrument. H<sub>2</sub>/Ar mixture (5% H<sub>2</sub>-95% Ar) was used as the reducing gas and heated at a heating rate of 10 °C/min from 30 to 850 °C with the flow rate of 30 mL/min.

#### 1.4 Activity test for ammonia synthesis

Catalytic performance evaluation was carried out in a continuous flow fixed-bed reactor (id = 14 mm). The catalyst bed was loaded in the isothermal zone of the reactor, and both the ends of the catalyst bed were filled with quartz with the size range of 1.0 ~ 2.0 mm to prevent the ammonia synthesis gas from channeling. The feed gas was derived from the decomposition of ammonia with deep removal of H<sub>2</sub>O, CO, CO<sub>2</sub> and residual NH<sub>3</sub> over Pd, 13 X, and 5 A molecular sieves and compressed by a compressor. Before catalyst activity test, the catalysts were reduced by the mixture of N<sub>2</sub> and H<sub>2</sub> (H<sub>2</sub> : N<sub>2</sub> = 3 : 1) according to the following temperature program: heating to 400 °C and standing for 4 h, then changing to 425 °C and standing for 6 h, then changing to 450 °C and standing for 10 h, and then changing to 475 °C and standing for 4 h, at the pressure of 5.0 MPa and space velocity of 30 000 h<sup>-1</sup>. Then, the activity was tested at the reaction temperature of 450, 425 and 400 °C, GHSV of 30 000 h<sup>-1</sup> and pressure of 15 MPa. In addition, to investigate the stability of the catalyst for ammonia synthesis, the catalyst was over heating at 500 °C for 15 h.

## 2 Results and discussion

### 2.1 Characterization of catalysts

The solid-state reaction of Fe(NO<sub>3</sub>)<sub>3</sub> · 9H<sub>2</sub>O with

oxalic acid can be expressed as the following equation (R1). According to the reaction, the pungent gas emission during milling should be HNO<sub>3</sub> and N<sub>2</sub>O<sub>5</sub>. This reaction is confirmed by the differential scanning calorimetry (DSC) experiments as demonstrated in Fig. 2.

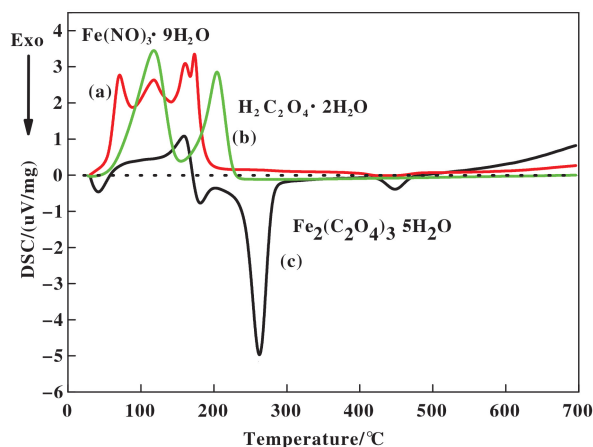
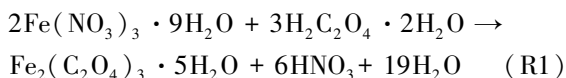


Fig. 2 DSC (differential scanning calorimetry) curves of (a) Fe(NO<sub>3</sub>)<sub>3</sub> · 9H<sub>2</sub>O, (b) H<sub>2</sub>C<sub>2</sub>O<sub>4</sub> · 2H<sub>2</sub>O and (c) Fe<sub>2</sub>(C<sub>2</sub>O<sub>4</sub>)<sub>3</sub> · 5H<sub>2</sub>O

As shown in DSC curves, clear endothermic peaks of dehydration and decomposition of Fe(NO<sub>3</sub>)<sub>3</sub> · 9H<sub>2</sub>O at temperatures between 50 ~ 200 °C were detected, while H<sub>2</sub>C<sub>2</sub>O<sub>4</sub> · 2H<sub>2</sub>O dehydrates and decomposes at 120 and 205 °C, respectively. These results are consistent with the reports in literature<sup>[30-31]</sup>. However, with the molar ratio of 3 : 2, once H<sub>2</sub>C<sub>2</sub>O<sub>4</sub> · 2H<sub>2</sub>O and Fe(NO<sub>3</sub>)<sub>3</sub> · 9H<sub>2</sub>O are well mixed, their decomposition behaviors differ from the pure components significantly. The DSC curve of the mixture is almost identical to that of Fe<sub>2</sub>(C<sub>2</sub>O<sub>4</sub>)<sub>3</sub> · 5H<sub>2</sub>O indicating the complete reaction of R1<sup>[32]</sup>. Unlike gas-phase reactions, solid-state is not limited by thermodynamics, resulting in complete formation of Fe<sub>2</sub>(C<sub>2</sub>O<sub>4</sub>)<sub>3</sub> · 5H<sub>2</sub>O<sup>[33]</sup>.



The morphologies of product of Fe<sub>2</sub>(C<sub>2</sub>O<sub>4</sub>)<sub>3</sub> · 5H<sub>2</sub>O and wüstite based catalysts are displayed in Fig. 3. Prior to the solid-state reaction, the pre-reduced wüstite-based catalyst exhibits smooth and clean surface (Fig. 3a). Following the solid-state reaction of Fe(NO<sub>3</sub>)<sub>3</sub> · 9H<sub>2</sub>O with H<sub>2</sub>C<sub>2</sub>O<sub>4</sub> · 2H<sub>2</sub>O in the presence

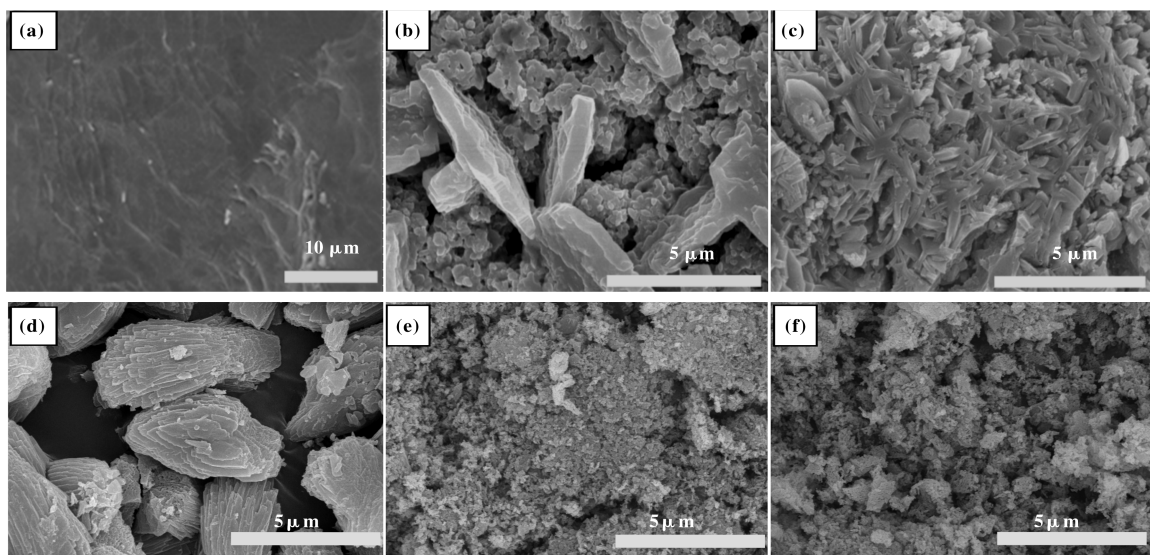


Fig. 3 SEM images of pre-reduced wüstite based catalysts before and after solid-state reaction and SEM images of  $\text{Fe}_2(\text{C}_2\text{O}_4)_3 \cdot 5\text{H}_2\text{O}$ , product of  $\text{Fe}_2(\text{C}_2\text{O}_4)_3 \cdot 5\text{H}_2\text{O}$  calcinated at different temperature.

(a) pristine pre-reduced wüstite catalyst, (b) pre-reduced wüstite catalyst after solid-state reaction, (c) calcination of sample (b) at 450 °C for 3 h, (d)  $\text{Fe}_2(\text{C}_2\text{O}_4)_3 \cdot 5\text{H}_2\text{O}$ , (e) product of  $\text{Fe}_2(\text{C}_2\text{O}_4)_3 \cdot 5\text{H}_2\text{O}$  calcinated at 400 °C and (f) product of  $\text{Fe}_2(\text{C}_2\text{O}_4)_3 \cdot 5\text{H}_2\text{O}$  calcinated at 450 °C.

of pre-reduced wüstite-based catalyst, it presents rough surface (Fig. 3b). Clearly, following solid-state reaction, the surface of pre-reduced wüstite based catalyst is fully covered by  $\text{Fe}_2(\text{C}_2\text{O}_4)_3 \cdot 5\text{H}_2\text{O}$  which is the major product of solid-state reaction. Moreover, the morphology of  $\text{Fe}_2(\text{C}_2\text{O}_4)_3 \cdot 5\text{H}_2\text{O}$  in presence of pre-reduced wüstite based catalyst differs from that of pure  $\text{Fe}_2(\text{C}_2\text{O}_4)_3 \cdot 5\text{H}_2\text{O}$  sample. Prior to the calcination, both morphologies of  $\text{Fe}_2(\text{C}_2\text{O}_4)_3 \cdot 5\text{H}_2\text{O}$  reveal assembling of sheet structure (Fig. 3b and 3d). Following calcination at 450 °C, the surface of pre-reduced

wüstite based catalyst is covered by cross-linked array of nanobelt (Fig. 3c). With the same treatment, pure  $\text{Fe}_2(\text{C}_2\text{O}_4)_3 \cdot 5\text{H}_2\text{O}$  decomposes into fine particles after calcination at 400 °C (Fig. 3e) or 450 °C (Fig. 3f). This difference attributes to the interaction between the pre-reduced wüstite-based catalyst and  $\text{Fe}_2(\text{C}_2\text{O}_4)_3 \cdot 5\text{H}_2\text{O}$  particles.

The XRD result of the solid-state reaction of  $\text{Fe}(\text{NO})_3 \cdot 9\text{H}_2\text{O}$  with  $\text{H}_2\text{C}_2\text{O}_4 \cdot 2\text{H}_2\text{O}$  in the absence of pre-reduced wüstite based catalyst confirms the formation of pure  $\text{Fe}_2(\text{C}_2\text{O}_4)_3 \cdot 5\text{H}_2\text{O}$  (Fig. 4a).

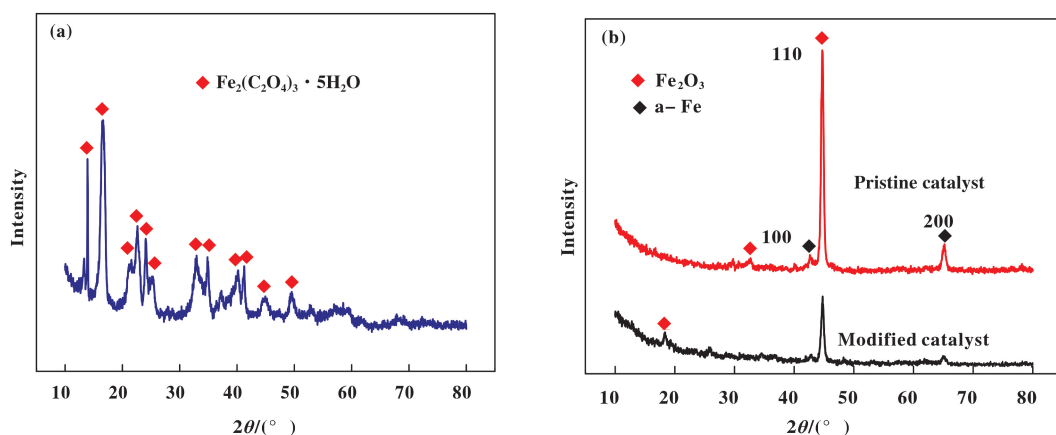


Fig. 4 XRD patterns of  $\text{Fe}_2(\text{C}_2\text{O}_4)_3 \cdot 5\text{H}_2\text{O}$  (a) and pre-reduced wüstite based catalyst before and after modification (b)

No impurity was detected by XRD pattern. In addition, weak diffraction peaks imply small crystal size of  $\text{Fe}_2(\text{C}_2\text{O}_4)_3 \cdot 5\text{H}_2\text{O}$  prepared by solid-state reaction.

The interaction is reinforced by the results of XRD experiments. As shown in Fig. 4b, XRD pattern of pristine pre-reduced wüstite based catalyst shows most  $\alpha\text{-Fe}$  formed which is the active phase for ammonia synthesis. The presence of  $\text{Fe}_2\text{O}_3$  is resulted from the surface oxidation during sample preparation for XRD experiment. The pre-reduced wüstite based catalyst was modified with  $\text{Fe}_2(\text{C}_2\text{O}_4)_3 \cdot 5\text{H}_2\text{O}$  (5% based on the Fe content in  $\text{Fe}_2(\text{C}_2\text{O}_4)_3 \cdot 5\text{H}_2\text{O}$ ) shows much weaker diffraction peaks of  $\alpha\text{-Fe}$ . Unlike XRD pattern of pure  $\text{Fe}_2(\text{C}_2\text{O}_4)_3 \cdot 5\text{H}_2\text{O}$  in Fig. 4a, no diffraction peaks of  $\text{Fe}_2(\text{C}_2\text{O}_4)_3 \cdot 5\text{H}_2\text{O}$  are observed, indicating that  $\text{Fe}_2(\text{C}_2\text{O}_4)_3 \cdot 5\text{H}_2\text{O}$  interacts with the surface of

pre-reduced wüstite based catalyst and disperses on the catalyst surface uniformly during solid-state reaction.

It is consistent with the results of TG as demonstrated in Fig. 5 and Fig. 6. The decomposition process

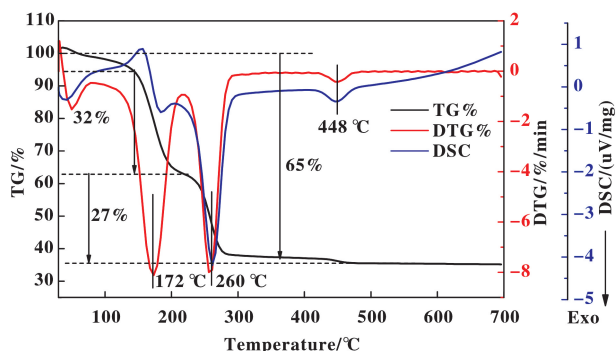


Fig. 5 TG and DTG experiments of  $\text{Fe}_2(\text{C}_2\text{O}_4)_3 \cdot 5\text{H}_2\text{O}$  prepared via solid-state reaction  $\text{Fe}(\text{NO}_3)_3 \cdot 9\text{H}_2\text{O}$  with  $\text{H}_2\text{C}_2\text{O}_4 \cdot 2\text{H}_2\text{O}$

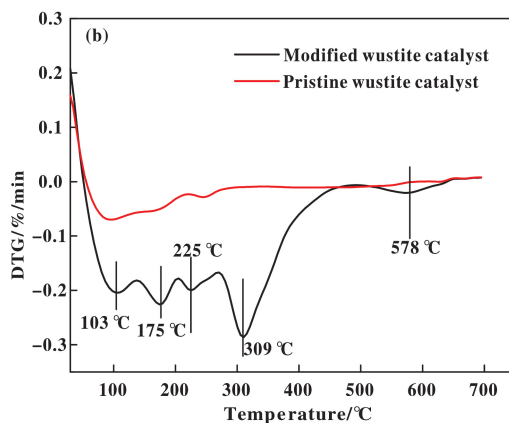
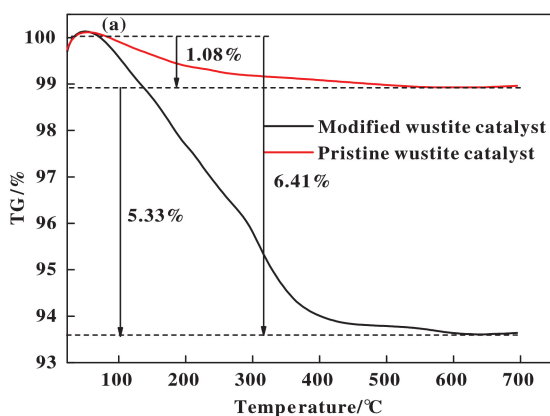
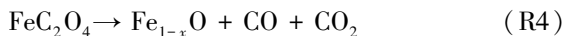
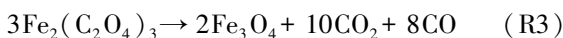
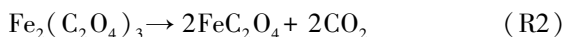


Fig. 6 TG and DTG experiments of wüstite based catalyst doped with  $\text{Fe}_2(\text{C}_2\text{O}_4)_3 \cdot 5\text{H}_2\text{O}$ . (a) TG, (b) DTG

of  $\text{Fe}_2(\text{C}_2\text{O}_4)_3 \cdot 5\text{H}_2\text{O}$  can be divided into three stages (R2 to R5).



As illustrated in Fig. 5, three peaks of DTG curve at 172, 260 and 448 °C correspond to reactions R2 and R3, reaction R4 and reaction R5, respectively. According to the DSC curve, endothermic and exothermic peaks around 170 °C can be assigned to reactions R2 and R3, respectively. Two exothermic peaks at 260 and 448 °C can be assigned to reaction of R4 and

R5, respectively. Moreover, the much weaker peak at 448 °C suggest that only very small amounts of iron oxide further decomposes into  $\text{Fe}_3\text{O}_4$  and Fe. In addition, the total weight loss of reactions R2-R5 (59%, 32% for reaction R2 and R3, 27% for reactions R4 and R5) agrees well with the calculated value (58.96%).

As shown in Fig. 6a, with the modification of 5% of Fe particles (based on the Fe content in  $\text{Fe}_2(\text{C}_2\text{O}_4)_3 \cdot 5\text{H}_2\text{O}$ ), the weight loss of modified wüstite-based catalyst is about 6.41%, which is much lower than that of calculated value (8.6%). We suggest that part of  $\text{Fe}_2(\text{C}_2\text{O}_4)_3 \cdot 5\text{H}_2\text{O}$  dehydrates and

decomposes during the drying process as the wet paste has to be dried after solid-state reaction. In addition, as displayed in Fig. 6b, decomposition of  $\text{Fe}_2(\text{C}_2\text{O}_4)_3 \cdot 5\text{H}_2\text{O}$  on pre-reduced wüstite based catalyst at temperatures of 175, 225, 309 and 578 °C. Compared with pure  $\text{Fe}_2(\text{C}_2\text{O}_4)_3 \cdot 5\text{H}_2\text{O}$  (in the absence of iron catalyst, Fig. 5), reaction temperatures of R2 and R3 split into two temperatures, from 172 to 175 and 225 °C. Especially, decomposition temperature of  $\text{FeC}_2\text{O}_4$  (R4) increases from 260 to 309 °C, suggesting the strong interaction between  $\text{FeC}_2\text{O}_4$  and pre-reduced wüstite based catalyst. The formation of new peak at 225 °C was caused by the weak interaction between  $\text{Fe}_2(\text{C}_2\text{O}_4)_3 \cdot 5\text{H}_2\text{O}$  and the surface of pre-reduced wüstite based catalyst. As a result, reaction temperature of R3 almost keeps unchanged after solid-state reaction in the presence of pre-reduced wüstite based catalyst. However, due to the interaction between  $\text{FeC}_2\text{O}_4$  and pre-reduced wüstite based catalyst, reaction temperature of R2 is elevated significantly. The shift of decomposition temperature of  $\text{Fe}_{1-x}\text{O}$  (R5) indicates the even stronger interaction with the surface of pre-reduced wüstite based catalyst. Clearly, these nano and micro particles derived from the decomposition of  $\text{Fe}_2(\text{C}_2\text{O}_4)_3 \cdot 5\text{H}_2\text{O}$  are significantly stabilized by this interaction. We suggest that it also plays a fundamental role in the performance of modified catalyst.

The  $\text{H}_2$ -TPR profiles shown in Fig. 7 represent the reduction behavior of pre-reduced wüstite based catalyst before and after modification. According to the results of  $\text{H}_2$ -TPR, reduction peaks of pre-reduced wüstite based catalyst before and after modification center around 519 and 537 °C, respectively. Clearly, with modification, the reduction temperature of pre-reduced wüstite based catalyst increased by 18 °C. In addition, for pre-reduced wüstite based catalyst, the starting reduction temperature is about 400 °C and the end temperature is about 600 °C, while the corresponding temperatures for modified pre-reduced wüstite based catalyst are 270 and 700 °C, respectively. The starting reduction temperature is 130 °C lower than pre-reduced wüstite based catalyst, which was attribute to

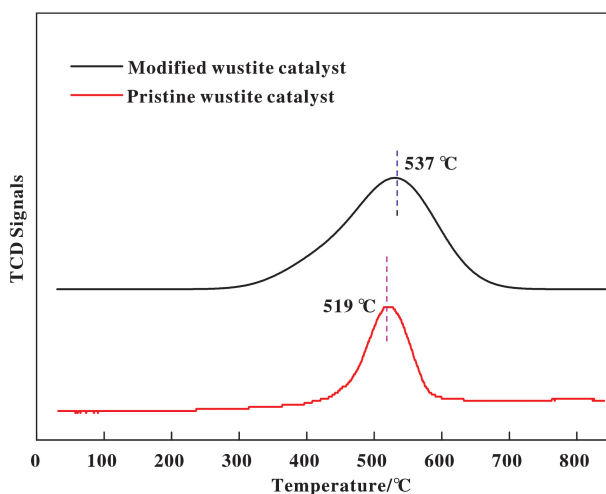


Fig. 7  $\text{H}_2$ -TPR patterns of pre-reduced wüstite based catalyst before and after modification

the reduction of surface or more dispersed  $\text{Fe}_2(\text{C}_2\text{O}_4)_3 \cdot 5\text{H}_2\text{O}$  over the catalysts. The end reduction temperature is 100 °C higher than pre-reduced wüstite based catalyst, which can be attribute to the strong interaction between modified Fe particles and pre-reduced wüstite based catalyst. In summary, the results of  $\text{H}_2$ -TPR indicate the formation of strong interaction between modified Fe particles and pre-reduced wüstite based catalyst, which was well agreed with TG and DTG (Fig. 6).

## 2.2 Catalytic activity

The activities of pristine and modified pre-reduced wüstite based catalyst for ammonia synthesis were evaluated at temperatures of 400, 425 and 450 °C, reaction pressure of 15 MPa and space velocity of 30 000  $\text{h}^{-1}$ . The results are summarized in Fig. 8(a).

With modification, the activity of pre-reduced wüstite based catalyst is enhanced significantly. It increases with Fe loading (neat Fe based on the Fe content in  $\text{Fe}_2(\text{C}_2\text{O}_4)_3 \cdot 5\text{H}_2\text{O}$ ) until the maximum activity is achieved at Fe loading of 5%. When loadings are higher than 5%, the activity of modified catalyst drops with loading. With the Fe loading of 5%, ammonia concentrations at the outlet of the reactor are improved from 12.4% to 15.6% at 450 °C, 11.0% to 14.8% at 425 °C and 9.4% to 13% at 400 °C, respectively. As iron catalyst for ammonia synthesis is a well consolidated catalyst with a development history of

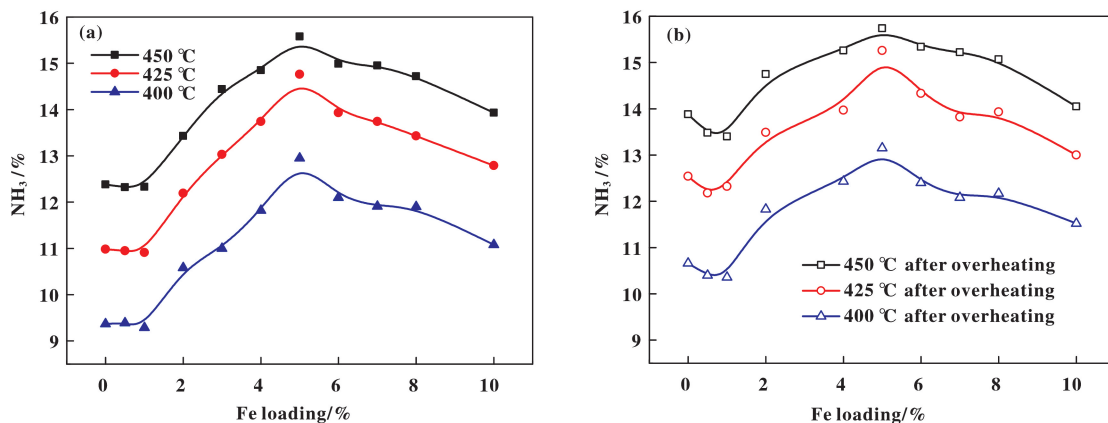


Fig. 8 Activity of pre-reduced wüstite based catalyst for ammonia synthesis at 15 MPa and space velocity of  $30\ 000\ \text{h}^{-1}$  (a) before over-heating and (b) after over-heating at  $500\text{ }^\circ\text{C}$  for 15 h.

more than 100 years, no further significant improvement is expected<sup>[4]</sup>. Therefore, the present work is a surprising progress on iron-based catalyst for ammonia synthesis. Via simple and one-step modification (solid-state reaction), the activity of pre-reduced wüstite based catalyst is enhanced by 25% to 38%. It is a significant progress for iron based catalyst for ammonia synthesis. With the Fe loading higher than 5%, we suggest that the surface of pre-reduced wüstite based catalyst is heavily covered by the particles. As we all know, in the absence of promoters, Fe is rather inactive for ammonia synthesis<sup>[34]</sup>. So with excessive amounts of nano and micro Fe particles, most doped Fe can not contact with promoters, while with small amounts of Fe doping, these particles are dispersed on the surface of pre-reduced wüstite based catalyst and interact with promoters located on the surface.

As demonstrated in Fig. 8 (b), modified wüstite based catalysts exhibit high stability for ammonia synthesis. After over heating at  $500\text{ }^\circ\text{C}$  for 15 h, identical activity was detected. Clearly, as mentioned previously, the strong interaction between nano and micro iron particles stabilizes the particles and prevent them from sintering.

### 3 Conclusions

Via simple and one-step modification (in-situ solid-state reaction of  $\text{Fe}(\text{NO}_3)_3 \cdot 9\text{H}_2\text{O}$  with  $\text{H}_2\text{C}_2\text{O}_4 \cdot 2\text{H}_2\text{O}$  in the presence of pre-reduced wüstite based cata-

lyst at room temperature), the activity of pre-reduced wüstite based catalyst is improved significantly. The solid-state reaction of  $\text{Fe}(\text{NO}_3)_3 \cdot 9\text{H}_2\text{O}$  with  $\text{H}_2\text{C}_2\text{O}_4 \cdot 2\text{H}_2\text{O}$  at room temperature yields  $\text{Fe}_2(\text{C}_2\text{O}_4)_3 \cdot 5\text{H}_2\text{O}$  completely and disperses on the surface of pre-reduced wüstite based catalyst. Following calcination or reduction, formed  $\text{Fe}_{1-x}\text{O}$  or Fe particles interact with the surface of pre-reduced wüstite based catalyst strongly, and thus stabilizes the nano and micro particles during reaction. As a result, high stability of catalyst is achieved. We propose it is a potential route for the improvement of ammonia synthesis catalyst and may be applied to other systems.

### References:

- [1] Horak J. 100 years of ammonia synthesis[J]. *Chem Lis*, 2015, **109**(3): 165–165.
- [2] Liu H Z. Ammonia synthesis catalyst 100 years: Practice, enlightenment and challenge[J]. *Chin J Catal*, 2014, **35**(10): 177–206.
- [3] Liu H Z, Li X N, Hu Z N. Development of novel low temperature and low pressure ammonia synthesis catalyst[J]. *Appl Catal A: Gener*, 1996, **142**(2): 209–222.
- [4] Pernicone N, Ferrero F, Rossetti I, *et al*. Wustite as a new precursor of industrial ammonia synthesis catalysts[J]. *Appl Catal A: Gener*, 2003, **251**(1): 121–129.
- [5] Han W, Yan H, Tang H, *et al*. Preparation of efficient ruthenium catalysts for ammonia synthesis via high surface area graphite dispersion[J]. *Rea Kine, Mecha Catal*, 2014, **113**(2): 361–374.

- [6] Lin B, Qi Y, Guo Y, *et al.* Effect of potassium precursors on the thermal stability of K-promoted Ru/carbon catalysts for ammonia synthesis[J]. *Catal Sci & Technol*, 2015, **5**(5): 199–204.
- [7] Ma Z, Xiong X, Song C, *et al.* Electronic metal – support interactions enhance the ammonia synthesis activity over ruthenium supported on Zr-modified CeO<sub>2</sub> catalysts [J]. *Rsc Adv*, 2016, **6**(56): 51106–51110.
- [8] Inoue Y, Kitano M, Kishida K, *et al.* Efficient and stable ammonia synthesis by self-organized flat Ru nanoparticles on calcium amide[J]. *ACS Catal*, 2016, **6**(11): 7577–7584.
- [9] Kitano M, Inoue Y, Ishikawa H, *et al.* Essential role of hydride ion in ruthenium-based ammonia synthesis catalysts[J]. *Chem Sci*, 2016, **7**(7): 4036–4043.
- [10] Kobayashi Y, Kitano M, Kawamura S, *et al.* Kinetic evidence: The rate-determining step for ammonia synthesis over electride-supported Ru catalysts is no longer the nitrogen dissociation step[J]. *Catal Sci & Technol*, 2017, **7**(1): 47–50.
- [11] Zybert M, Tarka A, Mierzwa B L, *et al.* Promotion effect of lanthanum on the Co/La/Ba ammonia synthesis catalysts - The influence of lanthanum content[J]. *Appl Catal A Gener*, 2016, **515**: 16–24.
- [12] Tarka A, Zybert M, Truszkiewicz E, *et al.* Effect of a barium promoter on the stability and activity of carbon-supported cobalt catalysts for ammonia synthesis [J]. *Chem Cat Chem*, 2015, **7**(18): 2836–2839.
- [13] Tsuji Y, Kitano M, Kishida K, *et al.* Ammonia synthesis over Co-Mo alloy nanoparticle catalyst prepared via sodium naphthalenide-driven reduction[J]. *Chem Commun*, 2016, **52**(100): 14369–14372.
- [14] Lendzion-Bielun Z, Jedrzejewski R, Ekiert E, *et al.* Heterogeneity of ingot of the fused iron catalyst for ammonia synthesis[J]. *Appl Catal A-Gen*, 2011, **400**(1/2): 48–53.
- [15] Figurski M J, Arabczyk W, Lendzion-Bielun Z, *et al.* On the distribution of aluminium and magnesium oxides in wustite catalysts for ammonia synthesis[J]. *Appl Catal A-Gen*, 2003, **247**(1): 9–15.
- [16] Jedrzejewski R, Lendzion-Bielun Z, Arabczyk W. The activity of fused-iron catalyst doped with lithium oxide for ammonia synthesis[J]. *Pol J Chem Technol*, 2016, **18**(2): 78–83.
- [17] Arabczyk W, Jasinska I, Jedrzejewski R. Iron catalyst for ammonia synthesis doped with lithium oxide [J]. *Catal Commun*, 2009, **10**(14): 1821–1823.
- [18] Yu X J, Lin B Y, Lin J X, *et al.* A novel fused iron catalyst for ammonia synthesis promoted with rare earth gangue[J]. *J Rare Earths*, 2008, **26**(5): 711–716.
- [19] Han W, Huang S, Cheng T, *et al.* Promotion of Nb<sub>2</sub>O<sub>5</sub> on the wustite-based iron catalyst for ammonia synthesis [J]. *Appl Surf Sci*, 2015, **353**: 17–23.
- [20] Lu Y H, Yang Y, Zhang T F, *et al.* Photoprompted hot electrons from bulk cross-linked graphene materials and their efficient catalysis for atmospheric ammonia synthesis [J]. *ACS Nano*, 2016, **10**(11): 10507–10515.
- [21] Martinez J M P, Carter E A. Thermodynamic constraints in using AuM (M = Fe, Co, Ni, and Mo) alloys as N<sub>2</sub> dissociation catalysts: Functionalizing a plasmon-active metal[J]. *ACS Nano*, 2016, **10**(2): 2940–2949.
- [22] Spencer N D, Schoonmaker R C, Somorjai G A. Structure sensitivity in the iron single-crystal catalysed synthesis of ammonia[J]. *Nature*, 1981, **294**(5842): 643–644.
- [23] Jacobsen C J H, Dahl S, Hansen P L, *et al.* Structure sensitivity of supported ruthenium catalysts for ammonia synthesis[J]. *J Mol Catal Chem*, 2000, **163**(1/2): 19–26.
- [24] Parker I B, Waugh K C, Bowker M. On the structure sensitivity of ammonia synthesis on promoted and unpromoted iron[J]. *J Catal*, 1988, **114**(2): 457–459.
- [25] Pelka R, Kielbasa K, Arabczyk W. The effect of size of crystallites on the nitriding process of the fused iron catalyst[J]. *Przem Chem*, 2010, **89**(4): 509–511.
- [26] Pelka R, Kielbasa K, Arabczyk W. The temperature effect on iron nanocrystallites size distribution[J]. *Curr Nanosci*, 2013, **9**(6): 711–716.
- [27] Arabczyk W, Ekiert E, Pelka R. Size-dependent transformation of alpha-Fe into gamma-Fe<sub>4</sub>N in nanocrystalline the Fe-NH<sub>3</sub>-H-2 system[J]. *J Phys Chem C*, 2016, **120**(32): 17989–17995.
- [28] Strongin D R, Carrazza J, Bare S R, *et al.* The importance of C7 sites and surface roughness in the ammonia synthesis reaction over iron [J]. *J Catal*, 1987, **103**(1): 213–215.
- [29] Jacobsen C J H, Jiang J, Mørup S, *et al.* Ammonia synthesis over multi-promoted iron catalysts obtained by high-energy ball-milling[J]. *Catal Lett*, 1999, **61**(3): 115–120.
- [30] Grigorie A C, Muntean C, Stefanescu M. Obtaining of  $\gamma$ -Fe<sub>2</sub>O<sub>3</sub> nanoparticles by thermal decomposition of polyethyleneglycol-iron nitrate mixtures[J]. *Thermochim Acta*, 2015, **621**: 61–67.

- [31] Kakumoto T, Saito K, Imamura A. Unimolecular decomposition of oxalic acid[J]. *J Phys Chem*, 1987, **91**(9): 2366-2371.
- [32] Gabal M A, El-Bellihi A A, Ata-Allah S S. Effect of calcination temperature on Co(II) oxalate dihydrate-iron(II) oxalate dihydrate mixture: DTA-TG, XRD, Mössbauer, FT-IR and SEM studies (Part II) [J]. *Mater Chem Phys*, 2003, **81**(1): 84-92.
- [33] Šesták J, Berggren G. Study of the kinetics of the mechanism of solid-state reactions at increasing temperatures [J]. *Thermochim Acta*, 1971, **3**(1): 1-12.
- [34] Kowalczyk Z, Jodzis S, Sroda J, *et al.* Influence of aluminium and potassium on activity and texture of fused iron catalysts for ammonia synthesis[J]. *Appl Catal Genet*, 1992, **87**(1): 1-14.

## 纳米-微米铁修饰的维氏体氨合成催化剂

李 蕾, 韩文锋\*, 李林辉, 刘化章\*

(浙江工业大学 工业催化研究所, 浙江 杭州 310014)

**摘要:** 我们以商业预还原的维氏体( $\text{Fe}_{1-x}\text{O}$ )氨合成催化剂为载体, 采用  $\text{Fe}(\text{NO})_3 \cdot 9\text{H}_2\text{O}$  和  $\text{H}_2\text{C}_2\text{O}_4 \cdot 2\text{H}_2\text{O}$  进行原位室温固相反应制备纳米铁或微米铁修饰的铁基氨合成催化剂, 并通过 XRD、SEM、TG-DTG、 $\text{H}_2$ -TPR 等进行了表征. 结果表明:  $\text{Fe}(\text{NO})_3 \cdot 9\text{H}_2\text{O}$  和  $\text{H}_2\text{C}_2\text{O}_4 \cdot 2\text{H}_2\text{O}$  室温固相反应完全生成产物  $\text{Fe}_2(\text{C}_2\text{O}_4)_3 \cdot 5\text{H}_2\text{O}$ , 且产物分散于载体维氏体催化剂表面. 通过纳米铁-微米铁的修饰, 催化剂的氨合成活性有很大提高且稳定性好. 催化剂活性随着 Fe 负载量的增加先增加后降低, 负载量 5% 时催化活性最好, 反应器出口氨浓由 450 °C (12.4%)、425 °C (11.0%)、400 °C (9.4%) 分别提升至 450 °C (15.6%)、425 °C (14.8%)、400 °C (13%). 通过一步简单的修饰, 维氏体催化剂的氨合成活性提高约 25% ~ 38%. 由于焙烧和还原, 生成的  $\text{Fe}_{1-x}\text{O}$  或铁粒子与铁催化剂表面发生强相互作用, 因此, 反应过程中纳米铁或微米铁粒子能稳定存在, 催化剂有较高的稳定性.

**关键词:** 氨合成; 固相反应; 维氏体; 修饰; 草酸铁